Available online at www.sciencedirect.com
ScienceDirect
Deep-Sea Research II 55 (2008) 582–593
DEEP-SEA RESEARCH PART II
www.elsevier.com/locate/dsr2

# Internal tides and vertical mixing over the Kerguelen Plateau

Young-Hyang Park[a,*], Jean-Luc Fuda[b], Isabelle Durand[a], Alberto C. Naveira Garabato[c]

[a]LOCEAN/USM 402, Département Milieux et Peuplements Aquatiques, Muséum National d'Histoire Naturelle, 43 rue Cuvier, 75231 Paris Cedex 05, France
[b]Centre Océanologique de Marseille, Campus de Luminy, 13282 Marseille Cedex 09, France
[c]School of Ocean and Earth Science, National Oceanography Centre, European Way, Southampton SO14 3ZH, UK

Accepted 14 December 2007
Available online 9 April 2008

**Abstract**

Within the context of the natural iron-fertilization study KEOPS, time series measurements of CTD and LADCP profiles at a site (50.6°S, 72°E; 528 m) coinciding with an annual phytoplankton bloom over the Kerguelen Plateau were made during the January–February 2005 KEOPS cruise. An important activity of highly nonlinear semidiurnal internal tides having peak-to-peak isopycnal displacements of up to 80 m is identified. These internal tides appear to be a principal agent for promoting elevated vertical mixing indispensable for upward transfer of iron within the seasonal thermocline. We estimate local vertical eddy diffusivities of the order of $4\times10^{-4}\,m^2\,s^{-1}$ using a Thorpe scale analysis. Although this estimate is higher by an order of magnitude than the canonical value $O$ $(0.1\times10^{-4}\,m^2\,s^{-1})$ in the open ocean away from boundaries, it is consistent with nonlinear internal wave/wave interaction theories, as verified by independent diffusivity estimates using the vertical wavenumber spectral methods for shear and strain. It is also suggested that the general ocean circulation may play an important role in preconditioning the bloom in that the relatively sluggish circulation over the shallow plateau (compared to the much more dynamic neighbouring deep ocean) may foster the bloom's observed annual recurrence over the plateau.


*Keywords:* Vertical diffusivities; Internal tides; Kerguelen Plateau

## 1. Introduction

The major objective of the physical component of the multidisciplinary KEOPS cruise conducted in January–February 2005 was the identification of the mechanism of natural iron fertilization over the Kerguelen Plateau. Iron availability is considered to be a limiting factor for the primary production in the Southern Ocean (Martin, 1990), which exerts an important influence on oceanic sequestration of atmospheric $CO_2$ and therefore climate. Satellite images of chlorophyll concentration consistently show two distinct regions of annual blooming or high primary productivity during the austral summer (Fig. 1). One region is found over the shallow shelf (<200 m) north of the Kerguelen Islands and the other over the shallow plateau (<500 m) south of the islands. The two areas are often separated clearly by a narrow band of low chlorophyll concentration, which is associated with the Polar Front (PF) skirting the southern edge of the islands whilst following the inner shelf edge between the 200 and 500 m isobaths (Park and Gambéroni, 1997; Park et al., 1998, 2002). The region north of the PF was studied by Blain et al. (2001), who related the high primary productivity to the enrichment of iron from two possible sources: (1) lithogenic inputs from the Kerguelen Islands and (2) inputs from bottom sediment. The most probable source of iron in the KEOPS region south of the PF may be the bottom sediment over the plateau, because direct lithogenic inputs from the islands are not likely to be important considering the general northward geostrophic flow in the area (Roquet et al., 2008; Park et al., 2008) and the presence of the PF possibly blocking any southward penetration of lithogenic inputs of Kerguelen Islands origin. Therefore, our working hypothesis for KEOPS is that the iron in the surface layer originates

*Corresponding author. Tel.: +33 1 40 79 31 70; fax: +33 1 40 79 57 56.
*E-mail address:* yhpark@mnhn.fr (Y.-H. Park).

0967-0645/$ - see front matter © 2008 Elsevier Ltd. All rights reserved.
doi:10.1016/j.dsr2.2007.12.027

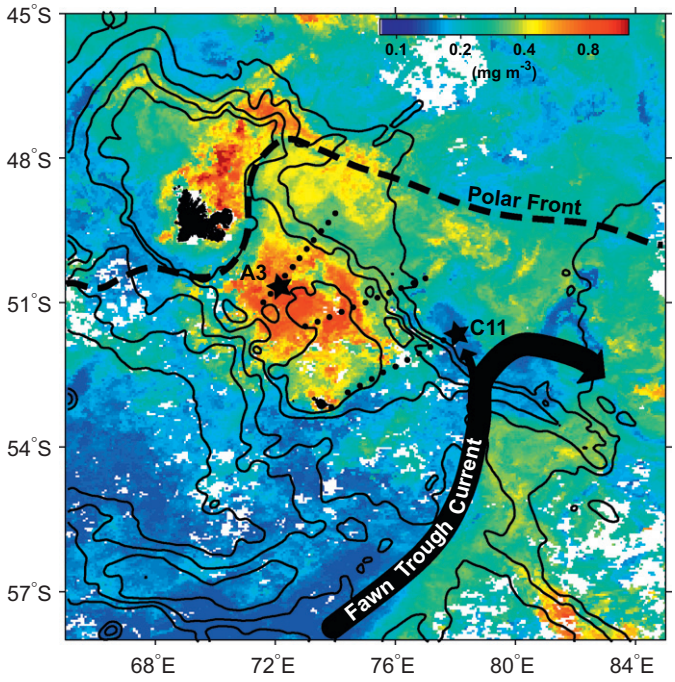


Fig. 1. Three hydrographic sections over the Kerguelen Plateau occupied during the KEOPS cruise in January–February 2005. A3 denotes the CTD and LADCP time series station at the bloom centre, while C11 is a contrasting bloom-free station. These stations are shown superimposed on the monthly mean chlorophyll concentration for January 2005 from MODIS data (courtesy of M. Mongin). The Polar Front from Park et al. (1998) and the Fawn Trough Current from Roquet et al. (2008) are shown.

from the iron-enriched bottom layer. With this premise, the key outstanding question is then: what is the primary mechanism for the upward transfer of iron within the water column?

Theories and observations (e.g., LeBlond and Mysak, 1978; Holloway and Merrifield, 1999; Merrifield et al., 2001) show that the interaction of a barotropic tidal current with the steep escarpment of a plateau can generate internal tides that propagate towards both the shallow region of the plateau and the deep ocean. In particular, intensive observations of internal tides together with fine- and microstructure measurements at the Hawaiian Ridge were recently made as part of the dedicated HOME (Hawaii Ocean Mixing Experiment) experiment (Rudnick et al., 2003; Levine and Boyd, 2006; Nash et al., 2006; Rainville and Pinkel, 2006). Intense internal tide activity over the Kerguelen Plateau also has been suggested by satellite altimetric measurements and numerical modelling of barotropic tides (Le Provost et al., 2001). This is consistent with the global baroclinic tidal model of Simmons et al. (2004), who present the Kerguelen Plateau as one of three major sites of internal tide generation in the Southern Ocean, together with Drake Passage and the Macquarie Ridge.

We thus put forward the hypothesis that internal tides may play a central role in transferring iron-enriched bottom water into the surface mixed layer, because high-mode internal tides should cascade into turbulence via nonlinear internal wave/wave interactions close to their generation site (Henyey et al., 1986; St. Laurent and Garrett, 2002; Polzin, 2004a, b), thereby sustaining enhanced vertical mixing throughout much of the water column. The iron transferred upward by this process would then accumulate in the surface layer during the winter season and promote the occurrence of the annual phytoplankton bloom in the following summer.

This hypothesis was tested during the KEOPS cruise. Specifically, our chief concern during KEOPS was the identification of internal tides and the estimation of the vertical eddy diffusivity, based on time series measurements of water properties and current profiles at a fixed point. The present paper reports our initial results on this topic. The hydrography and general circulation of the study area are documented in an accompanying paper (Park et al., 2008). A KEOPS synthesis article (Blain et al., 2007) highlights the greater efficiency of natural iron fertilization compared to previous short-term artificial iron-fertilization experiments in driving ocean productivity and carbon sequestration. In that paper, a diapycnal iron flux is estimated using our estimate of vertical diffusivity and the observed vertical gradient of dissolved iron (DFe) concentrations, together with discussions of the seasonal DFe budget in the Kerguelen Plateau area. In our Discussion section, we will elaborate on the latter subject by examining the circulation and residence time of water parcels over the plateau.

## 2. Observations of internal tides

### 2.1. Time series station A3

In order to identify internal tides a series of full-depth conductivity–temperature–depth (CTD) casts using a Sea-Bird 911-plus sounder were conducted at nominal time intervals of 2–3 h at station A3 (50°37′N, 72°05′E, bottom: 528 m). This station coincided with the centre of the annual bloom during the cruise period, in stark contrast to a "bloom-free" situation at station C11 (Fig. 1). Simultaneous measurements of horizontal current profiles were made using a lowered 300-kHz RDI acoustic Doppler current profiler (LADCP) attached to a CTD rosette sampler. The LADCP was configured with 10-m cells and 1-s sampling period, and data were post-processed using the Lamont Doherty Earth Observatory (LDEO) software package developed by Visbeck (2002). The repeated CTD and LADCP casts were occupied in two separate periods: one on 23–24 January spanning 21 h, and the other on 11–13 February spanning 38 h. Here we use mainly the 11–13 February data sets composed of 16 full-depth CTD and LADCP casts.

### 2.2. Evidence of internal tides from CTD data

The temporal evolution of property profiles at A3 clearly shows internal waves having a dominant semidiurnal

periodicity (Fig. 2). Peak-to-peak displacements of property isolines reach up to 80 m in the seasonal pycnocline found in the depth range of 80–180 m, between the surface mixed layer (<80 m) and the Winter Water (or subsurface temperature minimum layer) centred at 200 m. The amplitude of these vertical fluctuations decreases gradually towards the bottom mixed layer (>470 m). The conspicuous displacements within the seasonal pycnocline can be seen more vividly in ensembles of profiles of individual properties, in particular potential temperature and potential density (Fig. 3). Comparison of the internal tides observed at the two different time periods with a local tide table indicates that the intensity of internal tides at the A3 site is proportional to the strength of the barotropic tide at the Kerguelen Islands. In fact, the overall vertical displacements induced by internal tides during a spring tide (the second period considered here, 11–13 February) are about twice as large as those

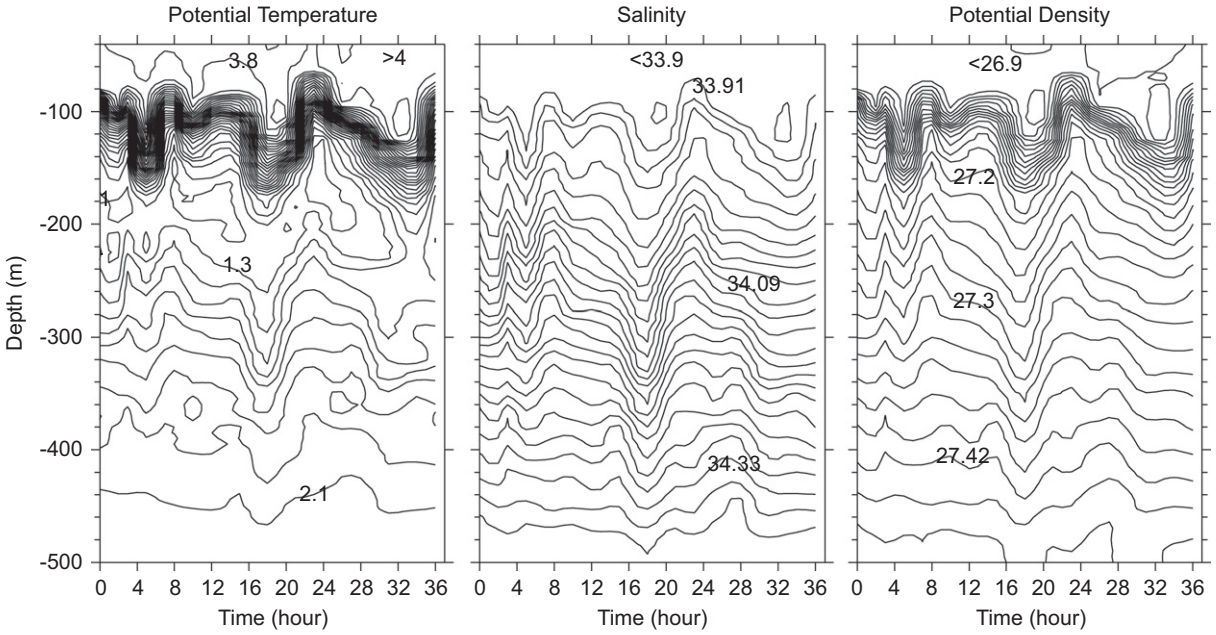


Fig. 2. Time–depth diagrams of potential temperature, salinity, and potential density at the time series station A3. Isolines are every 0.1°C for temperature, 0.02 for salinity, and 0.02 kg m$^{-3}$ for density, respectively.

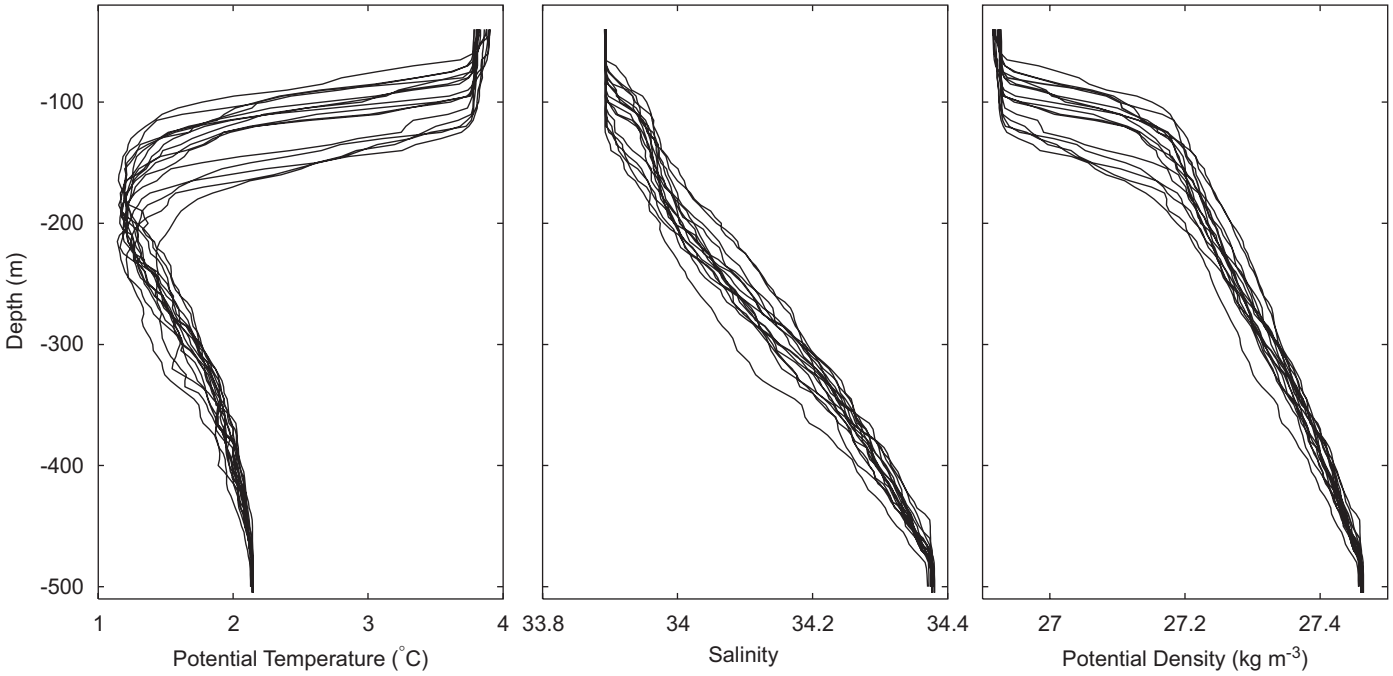


Fig. 3. Sets of ensemble profiles of potential temperature, salinity, and potential density at A3.

during a neap tide (the first period, 23–24 January) (not shown).

Closer examination of Fig. 2 indicates that the temporal evolution of property isoline displacements, especially in the seasonal pycnocline, is far from the sinusoid that would be expected from a simple monochromatic internal tide. Instead, the shape of the displacements is highly distorted by the presence of higher frequency waves and displays a complex asymmetric structure, often with a steep rise and a slow fall. These features are characteristics of nonlinear internal tides in shallow water (e.g., LeBlond and Mysak, 1978; Bowden, 1983; Park, 1986). Current spectra estimated from our recently recovered 1-year-long current meter mooring at two nearby sites (not shown) show several secondary peaks of higher harmonics such as the fourth diurnal $M_4$ ($T = 6.21$ h) and sixth diurnal $M_6$ ($T = 4.14$ h) constituents, supporting the idea of the local occurrence of shallow-water nonlinear effects.

### 2.3. Evidence of internal tides from LADCP data

The time series of LADCP velocity profiles at A3 confirm the dominance of semidiurnal currents at the site (Fig. 4). These can be decomposed into barotropic and baroclinic components, with the former representing the depth-averaged current and the latter the deviation from the barotropic component. The magnitude of the barotropic current is typically 15–20 cm $s^{-1}$. The corresponding progressive vector diagram suggests the existence of a weak northward mean flow (3 cm $s^{-1}$, 330°) superimposed on the dominant semidiurnal tidal oscillations (Fig. 5).

The baroclinic current time series (Fig. 4, bottom panel) also shows the predominant semidiurnal wave, with alternating opposite currents of the order of 10 cm $s^{-1}$ occurring across the seasonal pycnocline where the most intense vertical shear is apparent (see Fig. 6A). This is reminiscent of a characteristic time series of a first mode internal tide (LeBlond and Mysak, 1978; Park, 1986). However, the presence of a conspicuous irregularity in individual profiles as regards the change of amplitude and phase with depth is indicative of the presence of higher harmonics and higher vertical modes, which was already suggested by the afore mentioned property time series. A Fourier analysis of the time series data and their decomposition into vertical modes based on the linear internal wave theory could be made (e.g., Park, 1986), but

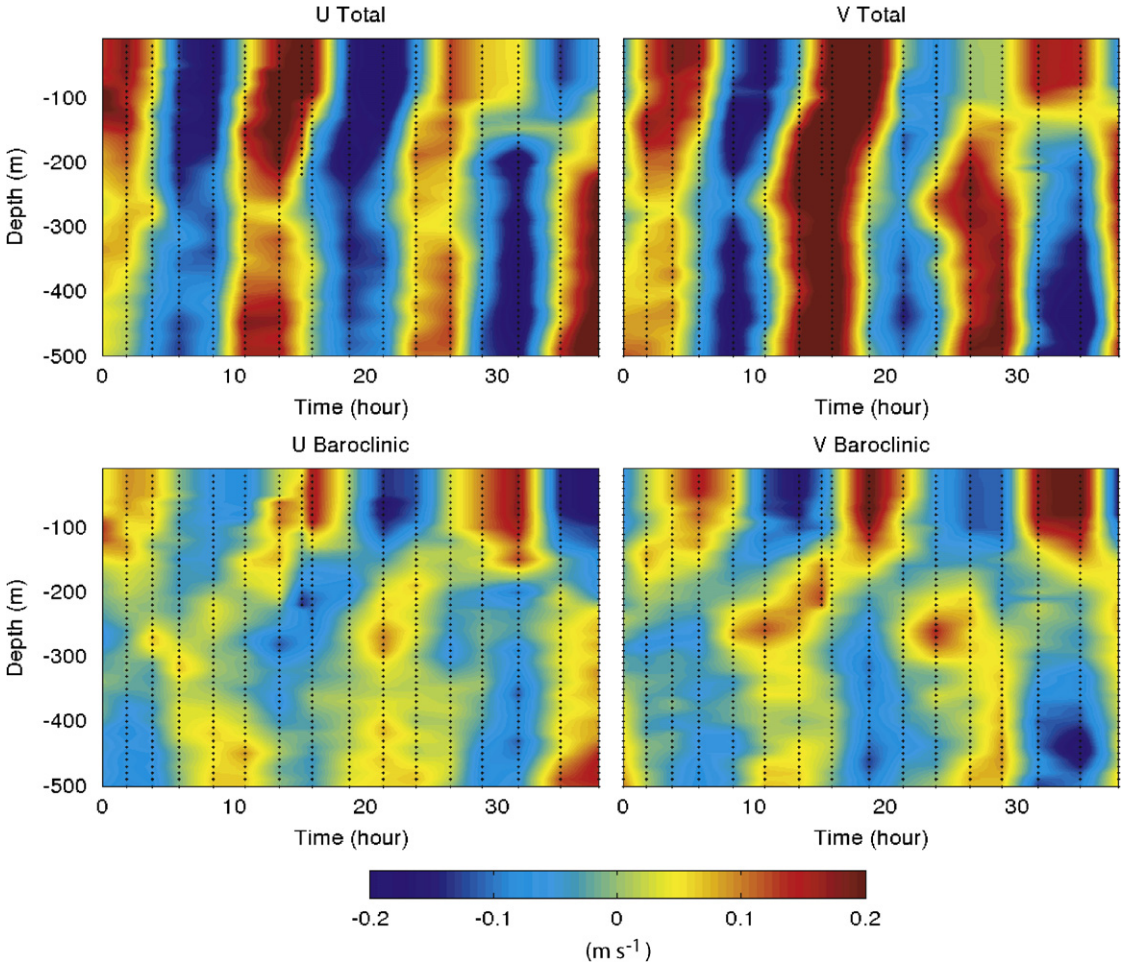


Fig. 4. (Top) Time–depth diagrams of total currents at A3 shown by their zonal ($U$ total) and meridional ($V$ total) components. (Bottom) Same as top panels, but for baroclinic currents calculated as the difference between the total currents and the barotropic currents shown in Fig. 5. Units are in m $s^{-1}$.

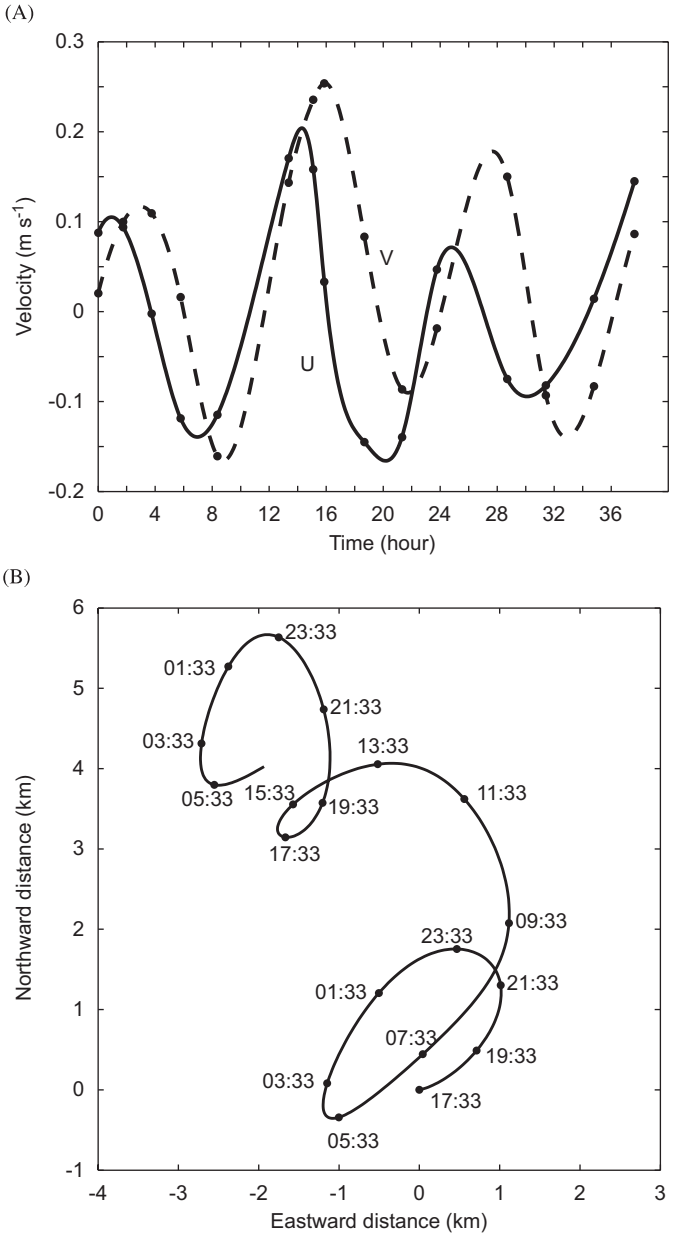


Fig. 5. (A) Temporal evolution of barotropic currents at A3 shown by their zonal (solid line) and meridional (dashed line) components. The original sparse data (dots) have been previously spline-interpolated before mapping. (B) Corresponding progressive vector diagram.

such is not deemed necessary in the context of the present study. It suffices to note that our LADCP data are qualitatively consistent with the CTD data in revealing dominant semidiurnal internal tides that are much distorted by superimposed higher frequency and higher vertical mode waves, yielding highly nonlinear internal tides.

## 3. Vertical eddy diffusivity

### 3.1. Estimates using the Thorpe scale method

We estimated the vertical eddy diffusivity $K_z$ at A3 using a Thorpe scale analysis. The Thorpe scale is a vertical length scale of turbulent overturning in a stratified flow (Thorpe, 1977). The calculation method consists of rearranging an observed potential density profile $\rho(z)$, which may contain inversions associated with turbulent overturns, into a stable monotonic profile without inversions. The vertical displacement necessary for generating the stable profile is the Thorpe displacement, and the Thorpe scale $L_T$ is defined as the root mean square of the Thorpe displacements within each overturn, which is identified as the vertical segment over which the sum of the Thorpe displacements drops back to zero (Dillon, 1982). The vertical eddy diffusivity is then defined as

$$K_z = \frac{\Gamma \varepsilon}{N^2}, \tag{1}$$

where $N = (-g\rho^{-1}\partial\rho/\partial z)^{1/2}$ is the Brunt-Väisälä frequency, $g$ is gravity, $\varepsilon$ is the rate of dissipation of turbulent eddy kinetic energy, and $\Gamma$ $(=0.2)$ is the mixing efficiency (Osborn, 1980). Using the definition of the Ozmidov length scale $L_O = (\varepsilon/N^3)^{1/2}$ (Ozmidov, 1965) and the empirical ratio of $L_O/L_T = 0.8$ (Dillon, 1982), $K_z$ can be written in terms of $L_T$ as

$$K_z = 0.128 L_T^2 N. \tag{2}$$

In estimating $L_T$, we followed a similar approach to that of Cisewski et al. (2005), who used the downcast CTD data averaged vertically over 0.4 m, but with an important exception for the supplementary treatment of data noise not considered by those authors. In fact, Eq. (2) implies that the reliability of $K_z$ estimates depends critically on that of $L_T$. It is therefore necessary to test whether inversions in density profiles are caused by genuine overturning motions, or by measurement noise and systematic errors caused by time-response mismatches in temperature and salinity sensors (Galbraith and Kelley, 1996). Another serious concern may be a possible contamination of CTD profiles by ship heave associated with surface-wave swell (Mauritzen et al., 2002), which is not the case here because the CTD winch of our R/V *Marion Dufresne* is equipped with a heave-compensation system, effectively damping ship heave (see Appendix A for details).

Our raw CTD data have a vertical resolution of about 0.033 m, as the CTD sampling and descent rates are 24 Hz and 0.8 m s$^{-1}$, respectively. The raw CTD profiles were first edited for apparent outliers exceeding $3\sigma$ (standard deviation) from a quadratic fit applied over successive segments of 20 m. The data were then averaged vertically over 0.4 m bins, with approximately 10 independent raw data points going into the average (Cisewski et al., 2005). This process can be considered as a low-pass filtering of the raw data, eliminating any instrumental noise or T–S mismatches having vertical wavelengths shorter than 0.4 m. In particular, the systematic errors due to T–S mismatches is likely to be negligible because the time constants of temperature and salinity sensors of the SeaBird 911-plus sounder we used are very small (0.04–0.06 s) and of the same order of magnitude (Cisewski et al., 2005). Although the short-term

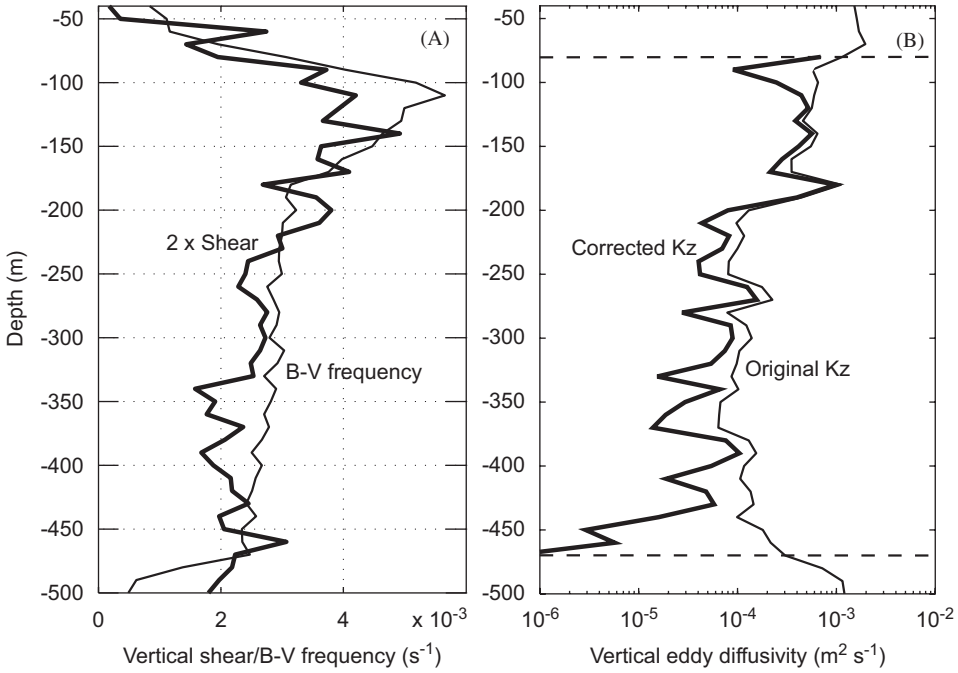


Fig. 6. (A) Set-mean profiles of vertical shear (thick line) and Brunt-Väisälä frequency (thin line) at A3. Shear values are shown multiplied by 2 for ease of comparison. (B) Set-mean profile of validated vertical eddy diffusivity (thick line) as compared to the original uncorrected estimates (thin line). Estimates have been previously averaged over 10-m bins before mapping.

mismatch between the temperature and conductivity sensors causing salinity spikes can be efficiently eliminated by this approach, there remains an issue with the long-term (tens of seconds) thermal inertia of the conductivity sensor (Lueck and Picklo, 1990), which has not been taken into account here.

The resulting smoothed profiles were reordered into gravitationally stable profiles, and Thorpe fluctuations $\rho'(z)$ were calculated as a difference profile between the initial and reordered profiles. By ensemble averaging individual standard deviations calculated from the afore mentioned 0.4 m segments of the entire profiles at A3 and C11, the average rms density error (DE) during KEOPS was estimated as DE$\sim$0.0005 kg m$^{-3}$. Any detectable signals due to turbulent overturns should satisfy at least the following two conditions. First, the overturn density interval $\Delta\rho_{OT}(=\rho_{max}-\rho_{min})$, which is greater than or equal to the maximum of $|\rho'(z)|$ within a given overturn, should be greater than 3DE at the 99% level of confidence:

$$\Delta\rho_{OT} > 3\mathrm{DE} = 0.0015\,\mathrm{kg\,m^{-3}}. \quad (3)$$

Second, the minimum overturn thickness $H_{min}$ should be at least the vertical distance separated by 3DE, i.e.

$$H_{min}(\mathrm{in\ m}) = 3\mathrm{DE}\left|\left(\frac{\partial\rho}{\partial z}\right)^{-1}\right| = \frac{3g\mathrm{DE}}{\rho_0 N^2} = \frac{1.5\times10^{-5}}{N^2}, \quad (4)$$

where $\rho_0$ is a representative mean density ($\sim10^3$ kg m$^{-3}$).

We used a sorting algorithm with ordering beginning at the shallowest depth. This yielded the depth range of each overturn, thus the overturn thickness $H$ and density interval $\Delta\rho_{OT}$, as well as the corresponding $L_T$, allowing us to estimate $K_z$ according to Eq. (2). For those depths where the above conditions for validating signals (Eqs. (3) and (4)) were not satisfied, the resulting $K_z$ values were considered invalid and replaced by zero. Consequently, the vast majority of overturns in the surface mixed layer ($z<80$ m) and the bottom mixed layer ($z>470$ m) were found to be invalid and were excluded from further calculations. The resulting set-averaged $K_z$ profile between 80 and 470 m (thick line) is shown in Fig. 6B, in comparison with the original profile obtained without signal validating constraints (thin line). Our new method yields conservative $K_z$ values with a point reduction by up to a factor of 3–4 on the mean, but below 450 m the reduction surpasses an order of magnitude. This is probably because both the signals and stratification below 450 m are too weak to pass frequently our validation criteria, rendering the results much less robust there.

The set- and depth-averaged corrected diffusivities at A3 are $3.8\pm2.4\times10^{-4}$ m$^2$ s$^{-1}$ in the seasonal pycnocline (80 m $<z<$ 180 m) and $0.8\pm1.1\times10^{-4}$ m$^2$ s$^{-1}$ in the deeper layer (180 m $<z<$ 470 m), as compared to their original values of $5.7\pm3.2\times10^{-4}$ and $1.5\pm1.4\times10^{-4}$ m$^2$ s$^{-1}$, respectively. Note that the enhanced vertical mixing in the seasonal pycnocline is significantly stronger than that in the deeper layer, which is likely to be related to the observed strongest shear in the upper layer due to nonlinear internal tides. Our $K_z$ value within the seasonal pycnocline far exceeds, by a factor of $\sim$40, the canonical

value ($0.1\times10^{-4}\,m^2\,s^{-1}$) in the mid-latitude open ocean away from boundaries (Gregg, 1987; Ledwell et al., 1993, 2000). It is also greater by a factor of ~4–14 than previous estimates below the surface mixed layer in other sectors of the Southern Ocean (Law et al., 2003; Naveira Garabato et al., 2004a; Cisewski et al., 2005).

For completeness, we applied the method also to station C11 where there are a total of eight CTD casts made at two different time periods. Here, we obtained the set- and depth-averaged diffusivities of $4.0\pm3.0\times10^{-4}\,m^2\,s^{-1}$ in the seasonal pycnocline and $5.8\pm3.9\times10^{-4}\,m^2\,s^{-1}$ in the deeper layer below 180 m. No significant difference between layers is observed here, and the vertical mixing in both layers is comparable in intensity to that in the seasonal pycnocline at A3. This is counter-intuitive considering the fact that there was no sign of a bloom at C11 (see Fig. 1). A possible explanation for this will be provided in the Discussion section.

### 3.2. Comparison with estimates using the vertical wavenumber spectral methods for shear and strain

In order to check further the reliability of our Thorpe scale-based diffusivities at A3, we tested two other indirect methods relying on the vertical wavenumber spectra for shear and strain (Polzin et al., 1995, 2002; Mauritzen et al., 2002; Naveira Garabato et al., 2004a, b). These methods parameterize the turbulent dissipation rate $\varepsilon$ in terms of the levels of internal wave shear and strain relative to the Garett and Munk (1975; GM) spectrum as modified by Cairns and Williams (1976). These are based on nonlinear internal wave/wave interaction theories (McComas and Muller, 1981; Henyey et al., 1986) linking the downscale transfer rate of kinetic energy in the internal wave field to the turbulence production. The combination of parameterizations for $\varepsilon$ and the traditional definition of vertical eddy diffusivity of Eq. (1) lead to the following types of semi-empirical formula for shear spectrum-based diffusivity $K_{sh}$ and strain spectrum-based diffusivity $K_{st}$ (Polzin et al., 1995; Mauritzen et al., 2002; Gregg et al., 2003; Naveira Garabato et al., 2004a, b):

$$K_{sh}=K_0\frac{\langle V_z^2\rangle^2}{{}_{GM}\langle V_z^2\rangle^2}F(R_\omega)G\left(\frac{f}{N}\right),$$

$$K_{st}=K_0\frac{\langle \zeta_z^2\rangle^2}{{}_{GM}\langle \zeta_z^2\rangle^2}F(R_\omega)G\left(\frac{f}{N}\right),$$

where $K_0=0.057\times10^{-4}\,m^2\,s^{-1}$; $\langle V_z^2\rangle$ and $\langle \zeta_z^2\rangle$ denote, respectively, the variance of the measured vertical shear and strain, each normalized by $N$; ${}_{GM}\langle V_z^2\rangle$ and ${}_{GM}\langle \zeta_z^2\rangle$ are the corresponding variables predicted by the modified GM model; and the two correction functions $F(R_\omega)$ and $G(f/N)$ are (e.g., Polzin et al., 1995; Naveira Garabato et al., 2004b):

$$F(R_\omega)=\frac{1}{a\sqrt{2R_\omega}}[-R_\omega+1+a^2+\{(R_\omega-1-a^2)^2+8R_\omega a^2\}^{1/2}]^{1/2}\quad\text{with}\quad a=\frac{f}{N},\tag{5}$$

$$G\left(\frac{f}{N}\right)=\frac{f\,\cosh^{-1}(N/f)}{f_{30}\,\cosh^{-1}(N_0/f_{30})},$$

where $R_\omega=\langle V_z^2\rangle/(N^2\langle \zeta_z^2\rangle)$ is the shear/strain ratio, and strain $\zeta_z$ is defined as the vertical derivative of isopycnal displacement and can be estimated as $\zeta_z=(N^2-\bar{N}^2)/\bar{N}^2$, with $\bar{N}$ being the time-mean or set-averaged profile of $N$; $R_\omega=3$ and $F(R_\omega)=1$ for the GM model; $f_{30}=f(30^\circ)=7.29\times10^{-5}\,s^{-1}$, $N_0=5.24\times10^{-3}\,rad\,s^{-1}$.

For our practical application of the methods, we followed the detailed procedures described in Naveira Garabato et al. (2004b) for $K_{sh}$ and Mauritzen et al. (2002) for $K_{st}$. Note that Polzin et al. (2002) give a detailed discussion on the LADCP transfer function, which has been applied here to estimate vertical wavenumber shear spectra and variance $\langle V_z^2\rangle$. In contrast to the finescale structure of the diffusivity profile estimated with the Thorpe scale approach, these methods only estimate an average spectrum over a finite depth interval of the order of a few hundred meters. With a later comparison with the former method in mind, we divided each shear and strain profile into three overlapping 320-m segments, beginning at 80 m and incrementing every 50 m: 80–400, 130–450, and 180–500 m. We excluded the surface mixed layer because the principal mixing agent there should be direct wind and buoyancy forcing rather than internal waves. Shear and strain variances were computed by integrating the corresponding vertical wavenumber spectra within a selected wavelength band ranging from a maximum of 320 m to a minimum of 80 m. Note that the selection of the latter wavelength is heuristic, but other values between 60 and 90 m do not change our results significantly.

The shear/strain ratio $R_\omega$ was estimated following the methodology described in Polzin et al. (1996), which reads:

$$R_\omega=\frac{\sum[((u_z-\bar{u}_z)^2+(v_z-\bar{v}_z)^2)/\bar{N}^2]}{\sum[(\bar{N}^2-N^2)/\bar{N}^2]^2},$$

where overbars represent an average over the 16 time series profiles at A3 and all other variables are estimates over 10 m. We averaged resulting $R_\omega$ values over the entire time series period and over successive 50-m segments beginning at 80 m depth, yielding ($R_\omega=0.43$, 0.62, 4.3, 4.6, 5.3, 2.1, 3.3, 2.6) for the depth bins (80–130, 130–180, 180–230, 230–280, 280–330, 330–380, 380–430, 430–480 m). As $R_\omega$ can be interpreted as the ratio of horizontal kinetic to available potential energy (Polzin et al., 1996, 2003), it is remarkable that the latter energy dominates ($R_\omega<1$) only within the seasonal pycnocline (80–180 m), which is in great contrast with deeper layers where $R_\omega$ values compare well with that of the $M_2$ internal tide at 50° latitude ($R_\omega=4.4$) (e.g., Polzin et al., 1995, Eq. (14)) or with the GM prescription ($R_\omega=3$). Mauritzen et al. (2002) attribute the enhanced strain variance observed within a section between the Ceara Rise and the continental slope off Brazil in the western equatorial Atlantic to quasi-permanent density

Table 1
Vertical eddy diffusivities (in $10^{-4}\,m^2\,s^{-1}$) at A3 estimated from three different methods: $K_z$ from the Thorpe scale method, $K_{sh}$ from the shear spectrum method, and $K_{st}$ from the strain spectrum method

| Depth segment | $K_z$ | $K_{sh}$ | $K_{st}$ | $R_\omega$ | $F(R_\omega)$ |
|---|---|---|---|---|---|
| $80\,m<z<400\,m$ | $1.9\pm1.6$ | $0.5\pm0.5$ | $1.4\pm1.8$ | 2.8 | 1.04 |
| $130\,m<z<450\,m$ | $1.4\pm1.6$ | $0.7\pm0.5$ | $0.1\pm0.1$ | 3.4 | 0.91 |
| $180\,m<z<500\,m$ | $0.8\pm1.1$ | $0.4\pm0.5$ | $0.1\pm0.1$ | 4.0 | 0.82 |
| Mean | $1.4\pm1.4$ | $0.5\pm0.5$ | $0.5\pm0.7$ | 3.3 | 0.92 |

Estimates of the shear/strain ratio $R_\omega$ and the $R_\omega$-related correction function $F(R_\omega)$ (Eq. (5)) are also given.

fine structure associated with vortical modes. In turn, Polzin et al. (2003) suggest several possible causes for the occurrence of excess strain relative to shear in the oceanic interior, which include (1) relatively more high-frequency internal waves at high vertical wavenumber, (2) the presence of shear instabilities characterized by low shear/strain ratio, and (3) increased finescale vortical mode variance at small scales. Although its potential contribution to our enhanced pycnocline strain cannot be ruled out, a rigorous discrimination of the quasi-permanent density fine structure from the high-frequency internal wave-induced strain is outside the scope of the present paper.

The shear- and strain-based diffusivity estimates are summarized in Table 1, in comparison with the Thorpe scale-based diffusivities $K_z$ previously averaged within the three selected depth segments. This table reveals several interesting points. First, $K_z$ values are systematically greater than $K_{sh}$ and $K_{st}$ estimates by a factor ranging from 2–4 with $K_{sh}$ to up to 14 with $K_{st}$, especially in segments below 130 m depth. Second, $K_{sh}$ values are relatively homogeneous among segments, while $K_{st}$ display a prominent maximum in the shallowest segment and a drastic drop by an order of magnitude in deeper segments. Third, because of this heterogeneity in $K_{st}$ values, their mean value over all segments is meaningless and misleading, although the latter value is coincidentally the same as that of $K_{sh}$, $0.5\times10^{-4}\,m^2\,s^{-1}$. For these reasons, we judge that the strain-based diffusivities may not be adequate for interpreting our observations, although there is no significant difference between $K_{st}$ and $K_z$ values in the shallowest segment. Aside from this, the Thorpe scale method is consistent with the shear spectrum method to within a factor of 2–4. This is just within the uncertainty of a factor of 3–4 proposed by Polzin et al. (2002) for the shear spectrum method using the spectrally corrected LADCP data. Also notable is that the segment-mean $R_\omega$ values decrease with decreasing depth, implying that waves with frequency higher than in a GM environment are most prolific near the seasonal pycnocline, as already mentioned. This is exactly what we have inferred from the time evolution of CTD and LADCP profiles.

## 4. Discussion

We have shown evidence of highly nonlinear internal tides with peak-to-peak amplitudes as high as 80 m over the shallow Kerguelen Plateau from repeated CTD and LADCP profiles gathered at time series station A3 during the KEOPS cruise. This occurrence at the bloom centre is associated with enhanced vertical mixing of $O(4\times10^{-4}\,m^2\,s^{-1})$ within the seasonal pycnocline, as verified by two independent indirect methods for estimating the vertical eddy diffusivity. As discussed below, these results appear to support our starting hypothesis concerning the dominant mechanism of vertical iron transfer. However, the estimated vertical mixing coefficients at station C11 where no significant bloom was observed are of the same order of magnitude as at A3, which would negate a simple linkage between the mixing intensity and the occurrence of a bloom. This apparent contradiction may be conciliated by taking the general circulation of the area into account, within the context of a simple advection-diffusion model of the phytoplankton concentration. In fact, time-mean surface currents over the plateau are weak (less than $5\,cm\,s^{-1}$), as shown not only by our LADCP data of limited duration at A3 (see Fig. 5B) but also by a 1-year-long current meter mooring deployed at a nearby site and the geostrophic velocity field derived from historical hydrographic data (Park et al., 2008). In contrast, currents in surrounding deep waters are much stronger often by a factor of 5 or more, especially in the Fawn Trough and its downstream area close to the eastern escarpment of the Kerguelen Plateau (Roquet et al., 2008; Park et al., 2008). Our chlorophyll-depleted station C11 is immersed in the latter flow environment. In other words, the highly productive shallow plateau is associated with weak mean currents, while the surrounding area of near-zero chlorophyll concentration is characterized by a strong mean flow. This suggests that, aside from a favourable upward iron flux due to internal tide-induced turbulent vertical mixing, the weak circulation over the plateau seems to provide a long retention time for nutrients and material concentration, thus enabling the development of a pronounced and relatively long-lasting bloom. In turn, in a strong current site such as C11, the advection of chlorophyll-depleted waters is likely to flush out the local primary producers, impeding any distinct concentration of chlorophyll to build up.

The apparent link between the weak circulation and high productivity over the Kerguelen Plateau may be understood in terms of a local retention of iron during the non-productive season, provided that the mean residence time over the plateau matches or exceeds that period. The flow below the surface mixed layer is very weak over the plateau, $<2\,cm\,s^{-1}$ (Park et al., 2008, Fig. 6), and displays an anticyclonic circulation pattern, passing first south of Heard Island and then veering to the northwest and skirting the 500 m isobath (Park et al., 2008, Fig. 7). This suggests that water parcels flowing from a point south of

the island to the northern part of the plateau where station A3 is located must travel a total distance of 400–500 km. This is indicative of a characteristic residence time of about 8–10 months, during which the diffusive flux of iron across the seasonal pycnocline can be stocked in the surface layer. This time scale is shown to be consistent with that derived from the seasonal DFe budget in the surface mixed layer at A3. In fact, Blain et al. (2007) estimate a vertical DFe supply of $1.4\times10^{-3}$ mmol m$^{-2}$ over 3 months of bloom via vertical mixing and a winter DFe stock utilisation of $4.7\times10^{-3}$ mmol m$^{-2}$. The former was calculated taking a mean vertical diffusivity of $3.2\times10^{-4}$ m$^2$ s$^{-1}$ (a little weaker than our final value of $3.8\times10^{-4}$ m$^2$ s$^{-1}$ presented here) and assuming a linear build up of vertical DFe gradients over 3 months in the 150–200 m depth stratum, while the latter is obtained from a seasonal DFe concentration difference multiplied by a mean mixed layer depth (~70 m). Note that the summer DFe concentration is $8.6\times10^{-5}$ mmol m$^{-3}$, as measured in the surface mixed layer, while the winter concentration is estimated as $15.3\times10^{-5}$ mmol m$^{-3}$, a value measured in the Winter Water layer at 200 m, below which the concentration increases gradually with depth to a maximum of $40.0\times10^{-5}$ mmol m$^{-3}$ at 500 m depth close to the bottom (Blain et al., 2007). If we assume that the vertical mixing rate that we derived in our summer survey is typical of the remainder of the year, then the winter DFe stock must have been achieved over ~10 months ( $=4.7/1.4\times3$). This value is close to the residence time estimated from knowledge of the circulation.

In the Introduction we advanced a pre-cruise hypothesis stating that sediments represent the dominant local source of iron. If we use a simple scaling analysis of a 1-D (vertical) diffusion equation, $\Delta C/T = K_z\Delta C/H^2$, the diffusive time scale $T$ ( $=H^2/K_z$) characterizing the transport of iron over $H=300$ m (from 500 to 200 m) by mixing at a rate of $K_z=3.8\times10^{-4}$ m$^2$ s$^{-1}$ is ~8 years. This value is an order of magnitude greater than the aforementioned residence time, as pointed out by a reviewer, which suggests that on an annual time scale, iron must originate from the deep-water layer immediately below the Winter Water and not directly from the local sediments. Thus we refine our hypothesis by stating that the long diffusive time scale of ~8 years applies to the shaping of the vertical distribution of DFe concentrations between 200 m and the seabed at ~500 m, while a much shorter diffusive length scale is likely associated with the transfer of iron across the base of the seasonal pycnocline. This can be easily verified by considering the seasonal DFe concentration difference of $\Delta C=6.7\times10^{-5}$ mmol m$^{-3}$ and the mean vertical DFe gradient of $8.2\times10^{-7}$ mmol m$^{-4}$ between 200 and 500 m, which yields a seasonal diffusive length scale of $H=82$ m. This length scale corresponds to a diffusive time scale of $T$~7 months, a value comparable to the mean residence time over the plateau derived above. In addition, Blain et al. (2007) note that about 50% of DFe consumed by phytoplankton in the bloom is not exported from the water column but is recycled by bacterial remineralization, which should replenish the water column's DFe pool. They also point out the need for an additional supply of iron (about one-third of the total) from the dissolution of lithogenic particulate Fe to close the DFe budget. This further strengthens our conjecture that iron may be feasibly supplied across the seasonal pycnocline by turbulent vertical mixing at a sufficiently high rate to support the annual bloom over the Kerguelen Plateau.

In the preceding discussion, we have regarded the iron budget over the Kerguelen Plateau to be essentially 1-D, and have considered turbulent mixing as the sole physical process controlling the vertical transfer of iron in the region. This has led to the realization that the local bottom source of iron at A3 is likely irrelevant to the observed bloom, as the associated diffusive time scale is much longer than the characteristic residence time of local waters. A critical depth horizon $H_c$ below which sediments may be considered as a relevant source of iron to the annual bloom may be estimated as $H_c$~340 m ( $=200+82+58$ m), where the three terms in the sum are the winter mixed layer depth, the seasonal diffusive length scale derived above (corresponding to a diffusive time scale of ~7 months using the vertical eddy diffusivity of $3.8\times10^{-4}$ m$^2$ s$^{-1}$ diagnosed here), and the bottom mixed layer thickness. The latter was estimated at A3 as the difference between the top of the bottom mixed layer (470 m) where frictional tidal mixing likely homogenizes near-bottom properties and the depth of the seabed (528 m). Thus, the observed annual recurrence of the bloom at A3 calls for a horizontal transport of iron from nearby source areas where the seabed is shallower than $H_c$. A detailed bathymetric map of the northern Kerguelen Plateau, given in our accompanying paper (Park et al., 2008, Fig. 1a), reveals that topography in the vicinity of A3 is both complex and sprinkled with many shallow (<300 m) seamounts, especially in the western part of the plateau south of A3 and in an extensive shoal around the McDonald/Heard Islands. These shallow submarine features stand out as the most plausible sources of iron to the intermediate layers of the water column at A3, where the nutrient may be advected horizontally by the weak anticyclonic mean circulation (Park et al., 2008) whilst diffusing vertically towards the surface mixed layer. In summary, both horizontal advection by the mean circulation and turbulent vertical diffusion appear to be indispensable for supplying iron to the A3 area, thus fuelling the recurrent annual plankton blooms over the Kerguelen Plateau.

This study emphasizes the importance of the joint action of advection by a sluggish mean circulation and intense turbulent vertical mixing for sustaining the spatially inhomogeneous primary productivity over the Kerguelen Plateau. We conjecture that this combination of physical processes may underlie the occurrence of recurrent blooms in the vicinity of other plateaux and islands of the Southern Ocean.

**Acknowledgements**

We thank the IPEV (Institut Polaire Français Paul-Emile Victor) for its financial and logistic support, and the captain, officers, and crew of the R/V *Marion Dufresne* for their professional assistance during the field experiment of KEOPS. Mathieu Mongin provided us with processed Modis satellite images of chlorophyll. We are also grateful for the financial support from the INSU (Institut National des Sciences de l'Univers) and the TOSCA program of the CNES (Centre National d'Etudes Spatiales). The Natural Environment Research Council (NERC) supported ACNG through a NERC Advanced Research Fellowship (NE/C517633/1). The original manuscript has been greatly strengthened by constructive comments of two anonymous reviewers.

## Appendix A. Diagnosis of ship heave effects on CTD profiles

In order to diagnose how ship heave associated with surface-wave swell is transmitted to the CTD package, a frequency spectrum of the time rate of change of pressure is calculated for each of the 16 repeated CTD casts at A3, and their average spectrum is shown in Fig. A1. The average descent rate of the package during these casts is $0.8\,\mathrm{m\,s^{-1}}$. Aside from the redness of the spectral shape for the lowest-frequency band ($f<0.01$ cps), which is irrelevant to ship heave, this pressure spectrum reveals two prominent peaks: one centred at $f=0.09$ cps and the other close to the high-frequency end, $f=10$ cps. The latter high-frequency ramp is likely to be associated with high-frequency noise in pressure at a level consistent with the pressure sensor's resolution, while the former peak at $f=0.09$ cps (corresponding to a periodicity of 11 s and a depth scale of 9 m using the mean package descent rate of $0.8\,\mathrm{m\,s^{-1}}$) should reflect the effect of surface swell. The latter depth scale associated with swell is greater than the Thorpe scale presented here, which may lead one to worry about whether our Thorpe scale estimate is contaminated or not. To dispel this concern, we estimated a vertical wavenumber spectrum of density gradient for each 100-m-long segment beginning at 80 m and using the 0.4-m-binned density profiles. A linear fit to the density gradient profile of each segment was removed prior to the spectral analysis, and Fig. A2 shows a mean spectrum averaged over the whole time series period in the seasonal pycnocline segment (80–180 m) as compared to that in the deepest segment (380–480 m). The other segments (not shown) are quite similar to the deepest segment. The spectrum in the seasonal pycnocline is slightly redder but far more energetic by an order of magnitude or more than its counterpart in the deepest segment that is completely flat. In both segments, no significant peak appears around the 0.11 cpm vertical wavenumber value, corresponding to a 9-m depth scale, suggesting that there is no evidence of a systematic contamination by swell. These results contrast with those of Mauritzen et al. (2002), who discard the Thorpe scale approach because of its possible contamination by swell in the western Atlantic. Note that the relatively large size of the *Marion Dufresne* (120 m length) compared to the Knorr (85 m) and the Oceanus (54 m) will tend to result in an averaging over all but the largest scales of the surface field, explaining why our Thorpe scale estimates tend to have better signal-to-noise ratios than the data examined by Mauritzen et al. Moreover, the CTD winch of the *Marion Dufresne* is equipped with a heave-compensation system, effectively damping the ship heave associated with swell, so the absence of contamination is not surprising.

To see this more clearly, we model the depth evolution $z(t)$ during a downcast as: $z(t)=c_0t+(1-\alpha)A\cos(2\pi ft)$, where $c_0$ represents a mean descent rate of the CTD package, $A$ is the swell amplitude, $f$ its frequency, and $\alpha$ a damping coefficient of a heave compensator. The contamination may occur if the package travels backward due to ship heave causing depth reversals, thus artificial mixing. This occurs if $\mathrm{d}z/\mathrm{d}t$ is negative, i.e., $c_0<2(1-\alpha)\pi fA\sin(2\pi ft)<2(1-\alpha)\pi fA$. A critical amplitude of swell $A_c$

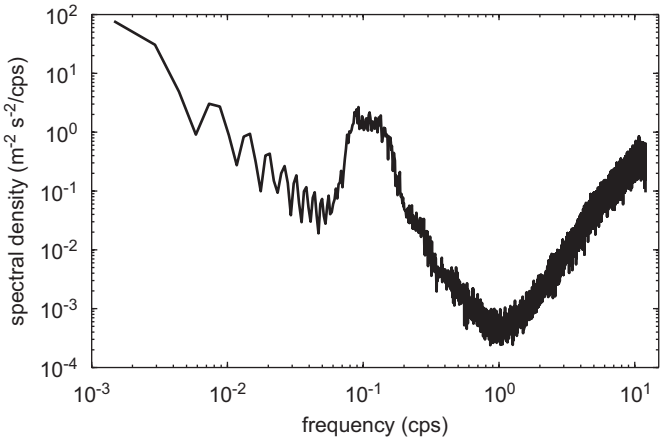


Fig. A1. Average frequency spectrum of the time rate of change of pressure from 16 repeated CTD casts at A3.

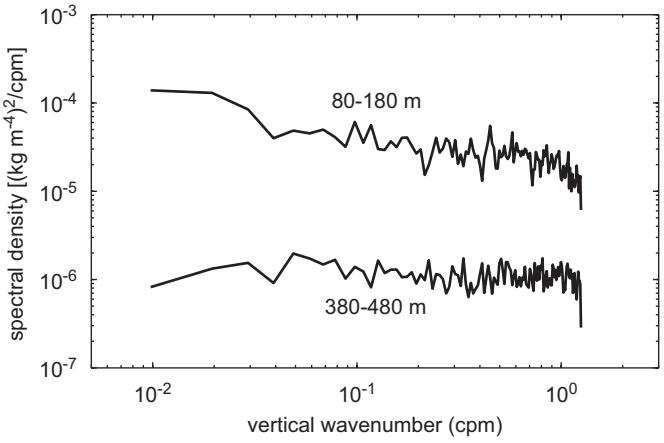


Fig. A2. Average vertical wavenumber spectra of density gradient in the 80–180 and 380–480 m depth segments from 16 repeated CTD casts at A3.

above which the contamination arises can then be defined as: $A_c = c_0/2(1-\alpha)\pi f$, which depends not only on the descent rate of the package $c_0$ and the period $(1/f)$ of swell but also more critically on the damping coefficient $\alpha$ of the heave compensator. In our case ($c_0 = 0.8\,m\,s^{-1}$, $f = 0.09\,s^{-1}$), $A_c = 1.4/(1-\alpha)\,m$. If our CTD winch were not equipped with a heave compensator (i.e., $\alpha = 0$), our CTD records would have been contaminated by swell having an amplitude of 1.4 m and greater, a situation commonly encountered in the Southern Ocean. According to the Neumann spectrum for a fully arisen sea, the maximum permissible amplitude of swell having a period of 11 s is about 8 m (Horikawa, 1978). We do not have precise information on $\alpha$ for the heave compensator of the *Marion Dufresne*, however, a damping efficiency of 83% would suffice to effectively prevent the CTD records from contamination of swell of whatever amplitude, as $A_c = 1.4/(1-0.83) = 8.2\,m$.

However, the effect of heave on the potential contamination of CTD data is not limited to the package reversal but also concern the problem associated with the package deceleration. Tool et al. (1997) note that when their CTD package decelerates, water entrained in the wake of the package can shoot forward past the sensors due to inertia, causing a double sampling of water. Although these effects are difficult to identify and remedy, we would like to briefly comment on some relevant aspects appearing in the aforementioned spectral analysis. Making reference to Fig. A1, the variance of the package descent rates associated with swell was estimated to be $0.125\,m^2\,s^{-2}$ by integrating the spectral density over the frequency range of 0.07–0.2 cps (or the wave period range of 5–14 s) where the quasi-totality of swell-related energy is concentrated. This suggests that the descent rate experienced overall fluctuations of $\pm 0.35\,m\,s^{-1}$ due to swell. As already noted, our CTD profiles were processed by binning and averaging over 0.4 m depth intervals, which is equivalent to an averaging over 0.5 s time intervals considering the mean descent rate of $0.8\,m\,s^{-1}$. The overshooting distance of water parcels due to package decelerations during this time interval should be less than 0.2 m ($>0.175 = 0.35 \times 0.5$) on average, suggesting that a substantial portion of those effects, if any, is expected to be much smeared by our 0.4 m data binning process.

Finally, because of its selective damping at low frequencies, the heave compensator does not exert any effect on the high-frequency noise. Consequently, the majority of depth reversals in raw CTD data are observed in a frequency band $f > 5$ cps (or at depth intervals less than 0.2 m). To minimize the contamination by such depth reversals during the initial data processing stage, we retained among several crossings of the same depth only the first crossing, discarding later crossings. In addition, any remaining contaminations and other undesirable high-frequency noise are largely eliminated by averaging CTD profiles over 0.4 m bins, as mentioned in the main text.

## References


Blain, S., Tréguer, P., Belviso, S., Bucciarelli, E., Denis, M., Desabre, S., Fiala, M., Martin-Jézéquel, V., Le Fèvre, J., Mayzaud, P., Marty, J.-C., Razouls, S., 2001. A biogeochemical study of the island mass effect in the context of the iron hypothesis. Kerguelen Islands, Southern Ocean. Deep-Sea Research I 48, 163–187.

Blain, S., Quéguiner, B., Armand, L., Belviso, S., Bombled, B., Bopp, L., Bowie, A., Brunet, C., Brussard, C., Carlotti, F., Christaki, U., Corbière, A., Durand, I., Ebersbach, F., Fuda, J.-L., Garcia, N., Gerringa, L., Griffiths, B., Guigue, C., Guillerm, C., Jaquet, S., Jeandel, C., Laan, P., Lefèvre, D., Lomonaco, C., Malits, A., Mosseri, J., Obernosterer, I., Park, Y.-H., Picheral, M., Pondaven, P., Remeny, T., Sandroni, V., Sarthou, G., Savoye, N., Scouarnec, L., Souhaut, M., Thuiller, D., Timmernans, K., Trull, T., Uitz, J., van-Beek, P., Veldhuis, M., Vincent, D., Viollier, E., Vong, L., Vagner, T., 2007. Effect of natural iron fertilization on carbon sequestration in the Southern Ocean. Nature 446.

Bowden, K.F., 1983. Physical Oceanography of Coastal Waters. Ellis Horwood, New York, 302pp.

Cairns, J.L., Williams, G.O., 1976. Internal wave observations from a midwater float: 2. Journal of Geophysical Research 81, 1943–1950.

Cisewski, B., Strass, V.H., Prandke, H., 2005. Upper-ocean vertical mixing in the Antarctic Polar Frontal Zone. Deep-Sea Research II 52, 1087–1108.

Dillon, T.M., 1982. Vertical overturns: a comparison of Thorpe and Ozmidov length scales. Journal of Geophysical Research 87, 9601–9613.

Galbraith, P.S., Kelley, D.E., 1996. Identifying overturns in CTD profiles. Journal of Atmospheric and Oceanic Technology 13, 688–702.

Garett, C.J.R., Munk, W.H., 1975. Space-time scales of internal waves: a progress report. Journal of Geophysical Research 80, 291–297.

Gregg, M.C., 1987. Diapycnal mixing in the thermocline: a review. Journal of Geophysical Research 92, 5429–5489.

Gregg, M.C., Sanford, T.B., Winkel, D.P., 2003. Reduced mixing from breaking of internal waves in equatorial waters. Nature 422, 513–515.

Henyey, F.S., Wright, J., Flatté, S.M., 1986. Energy and action flow through the internal wave field: an eikonal approach. Journal of Geophysical Research 91, 8487–8495.

Holloway, P.E., Merrifield, M.A., 1999. Internal tide generation by seamounts, ridges, and islands. Journal of Geophysical Research 104, 25,951–25,973.

Horikawa, K., 1978. Coastal Engineering: An Introduction to Ocean Engineering. University of Tokyo Press, 202pp.

Law, C.S., Abraham, E.R., Watson, A.J., Liddicoat, M.I., 2003. Vertical eddy diffusion and nutrient supply to the surface mixed layer of the Antarctic Circumpolar Current. Journal of Geophysical Research 108 (C8), 3272.

Le Provost, C., Carrere, L., Gaspar, P., Le Traon, P.E., Ponte, R., 2001. Ocean response to short-period atmospheric and tidal forcings. AVISO Newsletter 8, 75–77.

LeBlond, P.H., Mysak, L.A., 1978. Waves in the Ocean. Elsevier, New York, 602pp.

Ledwell, J.R., Watson, A.J., Law, C.S., 1993. Evidence for slow mixing across the pycnocline from an open-ocean tracer-release experiment. Nature 364, 701–703.

Ledwell, J.R., Montgomery, E.T., Polzin, K.L., St. Laurent, L.C., Schmitt, R.W., Tool, J.M., 2000. Evidence for enhanced mixing over rough topography in the Abyssal Ocean. Nature 403, 179–182.

Levine, M.D., Boyd, T.J., 2006. Tidally-forced internal waves and overturns observed on a slope: results from the HOME survey component. Journal of Physical Oceanography 36, 1184–1201.

Lueck, R.G., Picklo, J.J., 1990. Thermal inertia of conductivity cells: observations with a Sea-Bird cell. Journal of Atmospheric and Oceanic Technology 7, 756–768.

Martin, J.H., 1990. Glacial interglacial $CO_2$ change: the iron hypothesis. Paleoceanography 8, 1–13.

Mauritzen, C., Polzin, K.L., McCartney, M.C., Millard, R.C., West-Mark, D.E., 2002. Evidence in hydrography and density fine structure for enhanced vertical mixing over the Mid-Atlantic Ridge in the western Atlantic. Journal of Geophysical Research 107 (C103147).

McComas, C.H., Muller, P., 1981. The dynamic balance of internal waves. Journal of Physical Oceanography 11, 970–986.

Merrifield, M.A., Holloway, P.E., Johnston, T.M.S., 2001. The generation of internal tides at the Hawaiian ridge. Geophysical Research Letter 28, 559–562.

Nash, J.D., Kunze, E., Lee, C.M., Sanford, T.B., 2006. Structure of the baroclinic tide generated at Kaena Ridge, Hawaii. Journal of Physical Oceanography 36, 1123–1135.

Naveira Garabato, A.C., Polzin, K.L., King, B.A., Heywood, K.J., Visbeck, M., 2004a. Widespread intense turbulent mixing in the Southern Ocean. Science 303, 210–213.

Naveira Garabato, A.C., Oliver, K.I.C., Watson, A.J., 2004b. Turbulent diapycnal mixing in the Nordic seas. Journal of Geophysical Research 109 (C12010).

Osborn, T.R., 1980. Estimates of the local rate of vertical diffusion from dissipation measurements. Journal of Physical Oceanography 10, 83–89.

Ozmidov, R.V., 1965. On the turbulent exchange in a stably stratified ocean. Izvestiya Academy of Science, USSR, Atmosphere and Ocean Physics 1, 861–871.

Park, Y.-H., 1986. Semidiurnal internal tides on the continental shelf off Abidjan. Journal of Physical Oceanography 16 (9), 1585–1592.

Park, Y.-H., Gambéroni, L., 1997. Cross frontal injections of Antarctic Intermediate Water and Antarctic Bottom Water in the Crozet Basin. Deep-Sea Research II 44, 963–986.

Park, Y.-H., Charriaud, E., Ruiz Pino, D., Jeandel, C., 1998. Seasonal and interannual variability of the mixed-layer properties and steric height at station KERFIX, southwest of Kerguelen. Journal of Marine Systems 17, 233–247.

Park, Y.-H., Pollard, R.T., Read, J.F., Leboucher, V., 2002. A quasi-synoptic view of the frontal circulation in the Crozet Basin during the Antares-4 cruise. Deep-Sea Research II 49, 1823–1842.

Park, Y.H., Roquet, F., Durand, I., Fuda, J.L., 2008. Large scale circulation over and around the Northern Kerguelen Plateau. Deep-Sea Research II, this issue [doi:10.1016/j.dsr2.2007.12.027].

Polzin, K., 2004a. A heuristic description of internal wave dynamics. Journal of Physical Oceanography 34, 214–230.

Polzin, K., 2004b. Idealized solutions for the energy balance of the finescale internal wave field. Journal of Physical Oceanography 34, 231–246.

Polzin, K.L., Tool, J.M., Schmitt, R.W., 1995. Finescale parameterizations of turbulent dissipation. Journal of Physical Oceanography 25, 306–328.

Polzin, K.L., Oakey, N.S., Toole, J.M., Schmitt, R.W., 1996. Fine structure and microstructure characteristics across the northwest Atlantic Subtropical Front. Journal of Geophysical Research 101, 14,111–14,121.

Polzin, K.L., Kunze, E., Hummon, J., Firing, E., 2002. The finescale response of lowered ADCP velocity profiles. Journal of Atmospheric and Oceanic Technology 19, 205–224.

Polzin, K.L., Kunze, E., Toole, J.M., Schmitt, R.W., 2003. The partition of finescale energy into internal waves and geostrophic motions. Journal of Physical Oceanography 33, 234–248.

Rainville, L., Pinkel, R., 2006. Observations of the propagation and nonlinear interaction of the internal tide generated at the Hawaiian Ridge. Journal of Physical Oceanography 36, 1104–1122.

Roquet, F., Park, Y.-H., Guinet, C., Charrassin, J.-B., 2008. Observations of the Fawn Trough Current over the Kerguelen Plateau from instrumented elephant seals. Journal of Marine Systems, accepted for publication.

Rudnick, D.L., Boyd, T.J., Brainard, R.E., Carter, G.S., Egbert, G.D., Gregg, M.C., Holloway, P.E., Klymak, J.M., Kunze, E., Lee, C.M., Levine, M.D., Luther, D.S., Martin, J.S., Merrifield, M.A., Moun, J.N., Nash, J.D., Pinkel, R., Rainville, L., Sanford, T.B., 2003. From tides to mixing along the Hawaiian Ridge. Science 301, 355–357.

Simmons, H.L., Hallberg, R.W., Arbic, B.K., 2004. Internal wave generation in a global baroclinic tide model. Deep-Sea Research II 51, 3043–3068.

St Laurent, L.C., Garrett, C., 2002. The role of internal tides in mixing the deep ocean. Journal of Physical Oceanography 32, 2882–2899.

Thorpe, S.A., 1977. Turbulence and mixing in a Scottish Loch. Philosophical Transactions of the Royal Society of London Series A 286, 125–181.

Tool, J.M., Doherty, K.W., Frye, D.E., Millard, R.C., 1997. A wire-guided, free-fall system to facilitate shipborne hydrographic profiling. Journal of Atmospheric and Oceanic Technology 14, 667–675.

Visbeck, M., 2002. Deep velocity profiling using lowered acoustic Doppler current profiler: bottom track and inverse solutions. Journal of Atmospheric and Oceanic Technology 19, 794–807.